Quantification of bone healing

Comparison of QCT, SPA, MRI, and DEXA in dog osteotomies

Mark D. Markel[1], Mark A. Wikenheiser[1], Richard L. Morin[2], David G. Lewallen[1], and Edmund Y. S. Chao[1]

Four noninvasive imaging modalities were used to quantitatively evaluate and compare tibial osteotomy healing in dogs. Quantitative computed tomography (QCT), magnetic resonance imaging (MRI), single-photon absorptiometry (SPA), and dual-energy x-ray absorptiometry (DEXA) were the four techniques examined. Bilateral tibial osteotomies were performed in 32 dogs divided into four groups. The osteotomies were stabilized with a 2-mm gap using unilateral external skeletal fixation. Dogs were anesthetized, imaged with the four noninvasive techniques, and killed at 2–12 weeks. Invasive techniques were used to determine: 1) the torsional properties of the bone; and 2) the local stiffness properties and calcium content within the bone.

The techniques which had the strongest associations with the torsional properties of the osteotomies were QCT, SPA and DEXA. Generally, QCT and SPA had marginally stronger correlations than DEXA; but, overall, there were no differences between the techniques. MRI had the poorest associations with the torsional properties of the osteotomies. Generally, QCT had the strongest correlations with local material properties, such as indentation stiffness and calcium content. SPA had the second strongest correlations with calcium content and had the third strongest correlations with indentation stiffness behind DEXA. DEXA had the third strongest correlations for calcium content. With the exception of some of the correlations with indentation stiffness, MRI had the poorest associations with the local parameters studied.

The determination of bone material properties is a major field of interest both in orthopedics and in the study of metabolic bone disease (Mazess 1983). The orthopedic objectives include the diagnosis of normal and abnormal fracture healing patterns, the stress concentrating effects of bone tumors, recommendations for the removal of fixation devices, and optimization of implant design (Aro et al. 1989, McBroom et al. 1985). In metabolic bone diseases, techniques are needed for screening and diagnosis of patients with osteoporosis or metabolic conditions associated with bone loss such as renal osteodystrophy and hyperparathyroidism (Cann 1988, Eriksson et al. 1989, Mazess 1983).

We have compared three magnetic resonance imaging (MRI) sequences, quantitative computed tomography (QCT), single-photon absorptiometry (SPA), and dual-energy x-ray absorptiometry (DEXA) in their ability to quantitate the structural strength and local material properties of healing canine osteotomies and to determine which technique might have the greatest application in the evaluation of bone material properties.

Biomechanics Laboratory, Department of Orthopedics[1], and Department of Diagnostic Radiology[2], Mayo Clinic/Mayo Foundation, Rochester, Minnesota 55905, U.S.A.

Correspondence: Dr. Edmund Y.S. Chao.
FAX: (507) 284-5392

Material and methods

Thirty-two adult mixed-breed dogs were used. The dogs had a mean weight of 24 kg (17–34 kg) and were divided into four equal groups of eight dogs. Groups of dogs were noninvasively imaged and killed 2, 4, 8, or 12 weeks after surgery. Maturity was confirmed by radiographic examination for closure of the proximal tibial and distal femoral physes. Eight unpaired tibiae from random source dogs were used for determination of intact bone values.

Identical surgical procedures were performed on both hind limbs of each dog. Dogs were anesthetized with sodium pentobarbital (25 mg/kg, intravenously), placed in dorsal recumbency, and aseptically prepared and draped for surgery. A 5-cm skin incision extending through the periosteum was made over the medial diaphysis of the tibia. The periosteum was bluntly elevated over the circumference of the proposed osteotomy site. A middiaphyseal transverse osteotomy was made with an oscillating saw (Model 1370, Stryker Corp., Kalamazoo, MI). The osteotomy was stabilized (2-mm gap) using a small Orthofix unilateral external fixator (EBI Medical Systems, Inc., Fairfield, NJ; Figure 1). The incision was closed in three layers in routine fashion. Dogs were allowed to freely ambulate during the study period.

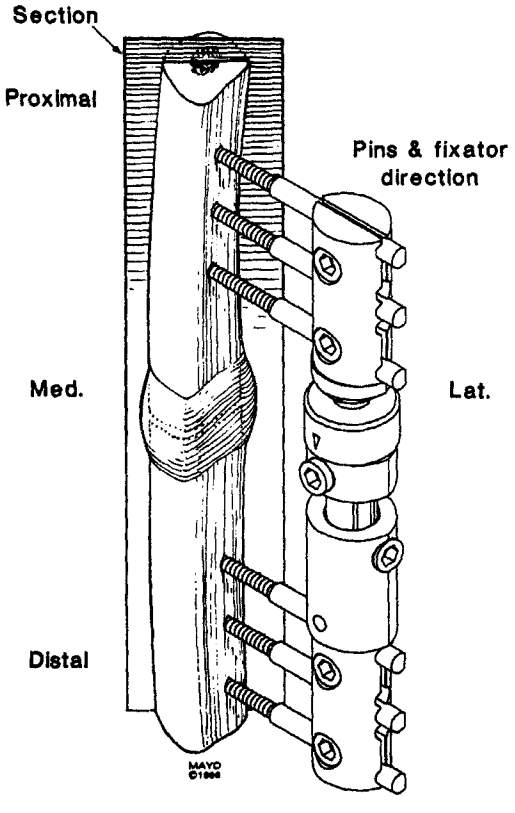

Figure 1. Orientation of osteotomy and external skeletal fixators.

New bone formation was quantitated with continuous tetracycline labeling (500 mg, orally, once daily) starting the day of surgery. This is less than the dose of 60 mg/kg that inhibits bone formation (Harris et al. 1968).

The dogs were anesthetized, the external fixators were removed, and MRI and QCT were performed. The dogs were then killed, the tibiae collected with the soft tissues intact, and SPA and DEXA performed. Tibiae were then analyzed for their torsional and local (indentation stiffness, calcium content, histologic parameters) material properties.

Noninvasive techniques

Radiographic analysis of callus

Craniocaudal and mediolateral radiographs were taken immediately after surgery to evaluate osteotomy reduction and pin placement and then biweekly until euthanasia.

The amount of radiographic periosteal callus formation was quantitated using a sonic digitizer. Periosteal callus formation was evaluated at the medial, lateral, cranial, and caudal cortices centered over the middle 3 cm of bone and expressed in units of area (mm^2). The callus area determined was normalized by dividing the amount of callus at each cortex by the total area of tibia centered over the middle 3 cm of bone.

MRI

A lucite calibration phantom was used to quantitate intensity values for the three different imaging techniques and to increase the inherent accuracy and repeatability of scanning (Jenkins et al. 1989). The phantom was curved to conform to the head coil of the scanner. Corn oil was selected as the normalization solution because of its stability in T_1 and T_2 weighted imaging.

Three scanning sequences were used to examine a 16-cm length of tibia including the osteotomy. Two multi-echo T_2 (TR 2000, TE 30, T_2W [1st echo]; and TR 2000, TE 60, T_2W [2nd echo]) and one T_1 (TR

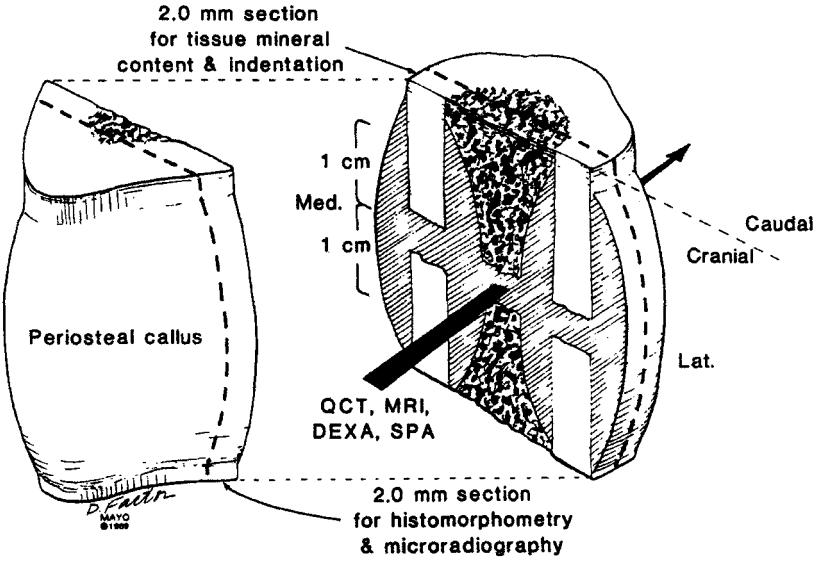

Figure 2. Illustration of orientation of noninvasive scans and of coronal sections for indendation testing, calcium content analysis, and microradiography.

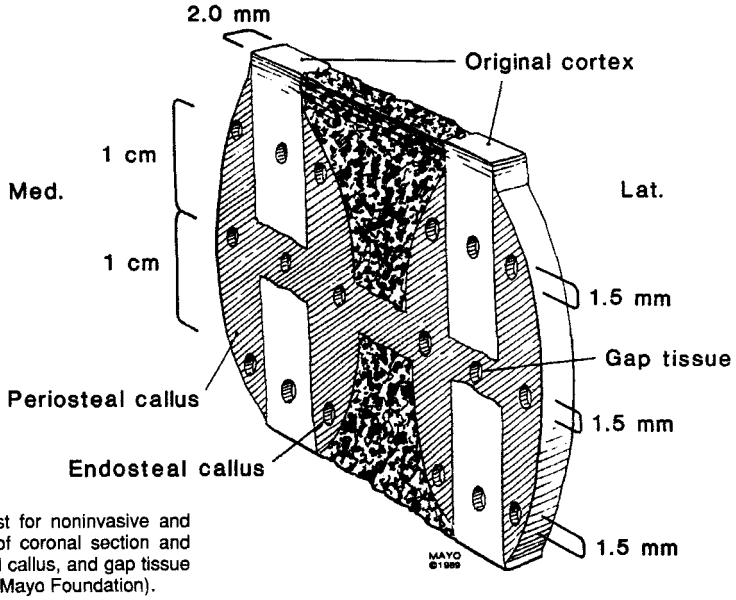

Figure 3. Eighteen regions of interest for noninvasive and invasive analysis. Note orientation of coronal section and location of periosteal callus, endosteal callus, and gap tissue (Markel et al. 1990a; by permission of Mayo Foundation).

500, TE 20, T_1W) weighted images were generated for both tibiae of each dog. All scanning was performed in the coronal plane (Figure 2). In the most centrally located coronal slice, 18 regions were analyzed for each bone: six areas of periosteal callus, six areas of endosteal callus, four areas of cortex, and two areas of gap tissue (Figure 3). The MRI scanner used for the procedure was a GE Signa 1.5 Tesla imager (General Electric, Medical Systems Department, Milwaukee, WI).

The scanning data were analyzed with a program designed to process biomedical images (Analyze®,

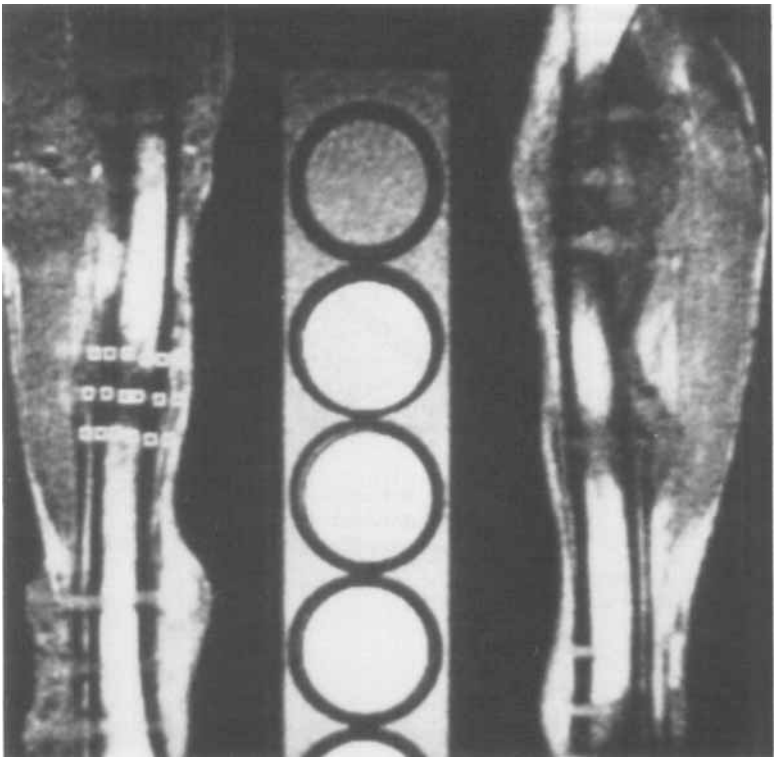

Figure 4. Coronal image of MRI demonstrating the 18 regions of interest analyzed for each bone.

Mayo Foundation, Rochester, MN; Figure 4). The bias (1024) was subtracted from all intensity values before data analysis or manipulation. The intensity of the 18 regions of interest were then normalized to the calibration solution.

QCT

A lucite calibration phantom was used to quantitate bone mineral density. The phantom was of the same type as that designed for quantitative assessment of trabecular bone content in the lumbar spine (Cann et al. 1985).

The table was set at a constant 115 cm. A frontal localization image was initially obtained, and a series of 27 contiguous 1.5-mm thick transverse scans were generated to include the middiaphysis between the innermost halfpins. The scanning length was 4 cm centered at the osteotomy gap.

Region-of-interest (1.7 cm^2, 100 pixels) measurements were obtained for each chamber of the phantom at the slice selected for QCT analysis (Figure 5). The CT number of each vial concentration was correlated with the vial's specific K_2HPO_4 concentration by linear least-squares regression. The 18 specific regions of interest described for MRI (0.07 cm^2, 4 pixels) were analyzed for each bone (Figure 3), although in the transverse plane. The CT scanner used for the study was a GE 9800 CT scanner (General Electric, Medical Systems Department, Milwaukee, WI).

SPA

SPA was performed after death on both tibiae of each dog with the soft tissues intact. The scan was performed using a prototype scanner which was designed and built by the Department of Nuclear Medicine and the Section of Engineering at the Mayo Clinic using ^{125}I as the radioactive source (Wahner et al. 1977). Each specimen with soft tissues intact was scanned in 7 cm of water using 2 mm rectilinear steps. The bone mineral content of the 18 specific sites were determined as described for MRI and QCT (Figure 3) from images generated by the scanning method.

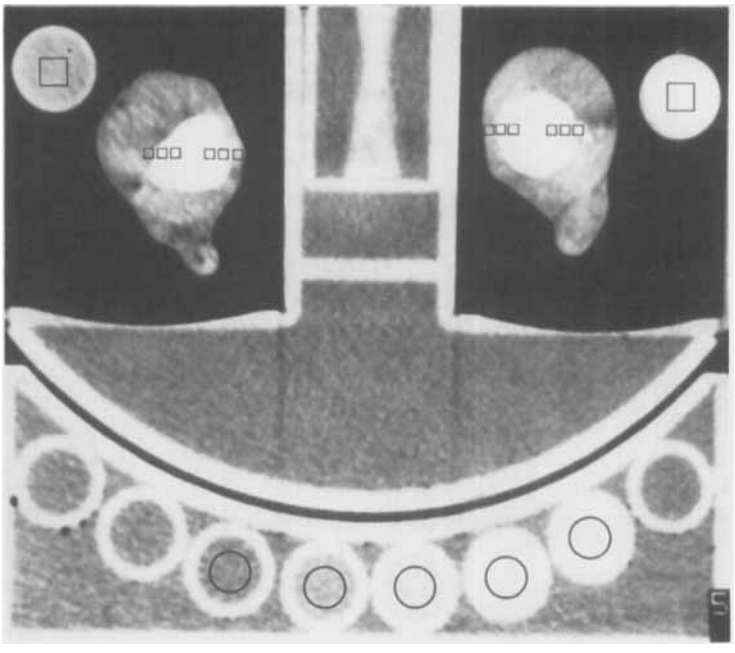

Figure 5. QCT scan demonstrating sampling sites in the transverse plane of the calibration solutions (bottom and solutions next to each tibia) and regions of interest within the bone volume.

DEXA

DEXA of both tibiae was performed with the soft tissues intact. The DEXA device uses a dual-energy x-ray source (70 kVp, 140 kVP) with a beam size of 2 mm (QDR 1000, Hologic, Inc., Waltham, MA). Both tibiae were placed in 20 cm of water and scanned in a proximal to distal direction for a length of 10 cm centered over the osteotomy site. Commercially available software was used to analyze the scanning data and determine the bone mineral content of the 18 regions of interest (Hologic, Inc., Waltham, MA) as described for QCT, MRI, and SPA (Figure 3) from images generated by the scanning method.

Torsional testing

Both tibiae of each dog were embedded in Wood's metal (Cerro-Bend Alloy) as previously described (Falkenberg 1961, Rand et al. 1981). Axial torsion with external rotation at a low strain rate (15° per min.) was applied to one randomly selected tibia of each dog on an Instron Electromechanical Testing Machine (Model 1125, Instron Corp., Canton, MA) until bone failure occurred. A low rate of loading was chosen to minimize inertial effects that may be present at fast loading (Burstein and Frankel 1971). Ultimate torque, torsional stiffness, energy absorption at failure, and angular deformation at failure were determined from the torque angular displacement curve. These data provide the structural strength of bone at different stages of osteotomy healing.

Indentation testing

A 2-mm thick coronal section centered over the fracture was cut for indentation testing and mineral content determination using a high-concentration diamond-wearing blade. Both of the remaining halves of bone were fixed in 70 percent alcohol within 5 hours of death for histologic and microradiographic analysis.

Indentation testing of the 18 specific sites was performed using an Instron Biaxial Testing Machine Model 1321. Sites were tested with a 1.5-mm diameter indentor with a half spherical testing surface of 1.5 mm diameter (Figure 6). The coronal sections were mounted on a rigid stage, and indentation was performed normal to the cut surface at a constant displacement rate of 2.75 mm per minute to a fixed depth of 0.375 mm. A low loading rate was used to obtain a static response. The slope of the linear portion of the curve, which is an index of the foundation stiffness of the bone, was measured.

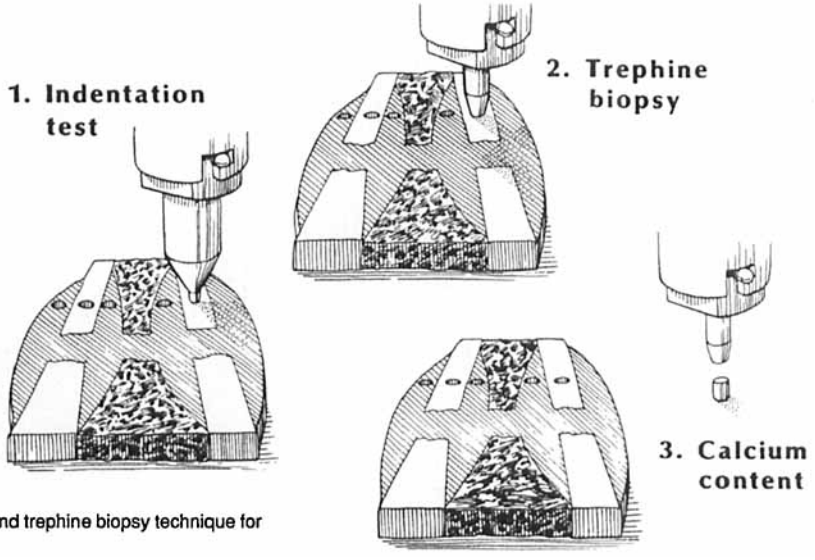

Figure 6. Indentation testing and trephine biopsy technique for calcium content analysis.

Tissue calcium content determination

The 18 regions of interest within the 2.0 mm by 30 mm unimbedded coronal section of each tibiae were analyzed for calcium content after indentation testing. A 1.5-mm diameter trephine was used to sample the exact site used for indentation testing (Figure 6). The samples were weighed, dried in a 100 °C oven for 48 hours. The samples were then dissolved in concentrated HNO_3 for 48 hours. The mineral content of the resultant solution was determined by an inductively coupled plasma atomic-emission spectroscopy technique (Nixon et al. 1986). Data were calculated as mg $[Ca^{++}]$/g dry weight of tissue.

Microradiography and histology

The bone halves remaining after indentation testing were fixed in 70% alcohol and dehydrated in increasing concentrations of alcohol (Baron et al. 1979). The bones were embedded in methyl methacrylate and cut in the coronal plane to an undecalcified bone section width of 200 μm using a low-speed diamond saw, and the 200-μm specimens were ground to the desired thickness of 98-100 μm between two pieces of plate glass roughened with #120 grit carborundum.

Microradiographs of the coronal section were made using high resolution contact film (Kodak spectroscopic plates, Eastman Kodak, Rochester, NY) according to Jowsey et al. (1965) and Kelly et al. (1959).

Bone porosity was quantitated with a semi-automated computerized image analyzer including a video image processor (Datacube, Inc., Peabody, MA) with a microscope and custom-made software. The porosity of periosteal and endosteal callus and gap tissue were expressed as a percentage of the total new bone area. The intracortical porosity was expressed as a percentage of the total bone area. This method has been verified in our laboratory (Aro et al. 1989, Lewallen et al. 1988). Porosity was measured for each area of the 18 specific sites.

The rate of new bone formation was studied by a tetracycline labeling technique using point counting (Frost 1979, Vanderhoeft et al. 1967). The amounts of the new bone, porosity, and unlabeled cortical bone were expressed on a percentage basis of each region of interest. Therefore, at each specific cortical site, new bone formation, original unlabeled bone, and porosity were measured. In the gap tissue and callus sites, there was no original bone, so only new bone formation and porosity were calculated.

Data analysis

The mean value for the six sites of periosteal callus, the six sites of endosteal callus, the four sites of cortex, and the two sites of gap tissue were determined for each tibia with each of the four imaging techniques. Paired comparisons using a Student's *t*-test between the right and left limb were performed for

each of these four types of tissue, and the results of the two limbs were averaged.

The association between the mean values quantitated from the six different imaging techniques (MRI [T_1W, T_2W (1st echo), T_2W (2nd echo)], QCT, SPA, and DEXA) and indentation stiffness, calcium content, ultimate torque, torsional stiffness, energy to failure, and angular deformation at failure were quantitated with least-squares regression. Data were correlated for each specific tissue (periosteal, endosteal, gap, and cortex) with 32 independent points (one for each dog) per correlation.

The six noninvasive imaging methods (three MRI, QCT, SPA, and DEXA) were compared by performing repeated measures ANOVA on the residual components of each least squares regression. If repeated measures ANOVA revealed differences between the residual components of the noninvasive techniques, Tukey's studentized range post-hoc *t*-test was performed. Therefore, the noninvasive technique which had the strongest association with each of the specific dependent variables was calculated.

All differences were considered significant at a probability level of 95 percent ($p < 0.05$). All statistical analyses were performed with a commercially available software program (SAS Institute, Inc., Cary, NC).

Results

Osteotomy healing properties

The two-week osteotomies deformed in torsion but did not fracture, so ultimate torque, energy absorption at failure, and angular deformation at failure could not be determined (Table 1). The ultimate torque and torsional stiffness of the osteotomies increased as polynomial functions over time and were weaker than intact bone specimens at 12 weeks. Energy absorption at failure increased as a logarithmic function over time and was greater than intact bone specimens at 12 weeks. Angular deformation at failure did not differ from intact bone at any time interval.

Local indentation stiffness of gap tissue increased linearly over time (Table 2). In periosteal tissue, stiffness increased as a power function up to eight weeks and then plateaued at 12 weeks. Endosteal stiffness peaked at 8 weeks and then decreased by 12 weeks. Cortical stiffness decreased over time.

The calcium content of gap tissue, periosteal callus, and endosteal callus increased over time (Table 2). The mathematical models to describe dry weight calcium's change over time were linear for periosteal, endosteal, and gap tissue. There were no changes in cortical calcium content over time (Table 2).

The fraction of unlabeled cortical bone decreased as a log function overtime. New bone formation peaked in periosteal and endosteal callus at four-weeks and then plateaued (periosteal) or declined (endosteal) by 12 weeks (Table 2, Figure 7). In gap tissue and cortical bone, new bone formation increased as a power function over time. Porosity decreased and plateaued in periosteal callus, whereas endosteal callus porosity increased to greater than two-week values by 12 weeks. The porosity of gap tissue decreased as a power function with time but plateaued between 8 and 12 weeks.

Radiographic callus formation peaked at six weeks and then gradually decreased. At all time intervals, the lateral callus was greater than the medial, cranial, and caudal callus, with the medial callus always the smallest.

Table 1. Torsional properties of healing osteotomy. Mean *SEM.* (Markel et al. 1990a)

Weeks after surgery	Ultimate torque (Nm)		Torsional stiffness (Nm/rad)		Energy[1] (Joules)		Rotation[2] (degrees)	
Intact bone	28.5[a]	*2.3*	163.6[a]	*15.3*	3.7[a]	*0.3*	13.0[a]	*0.5*
2	...	...	0.9[b]	*0.2*	....	...	...	...
4	3.6[b]	*0.7*	22.3[b,c]	*9.8*	3.3[a]	*0.8*	15.9[a]	*3.7*
8	15.6[c]	*2.1*	77.5[d]	*10.5*	11.5[b]	*2.5*	13.9[a]	*0.9*
12	12.2[c]	*1.5*	54.8[d]	*7.6*	12.4[b]	*4.3*	16.8[a]	*2.5*

[1] Energy absorption at failure.
[2] Angular deformation at failure.
[a–d] Means within a column with superscripts of differing letters differed from each other ($p < 0.05$).
... Not applicable.

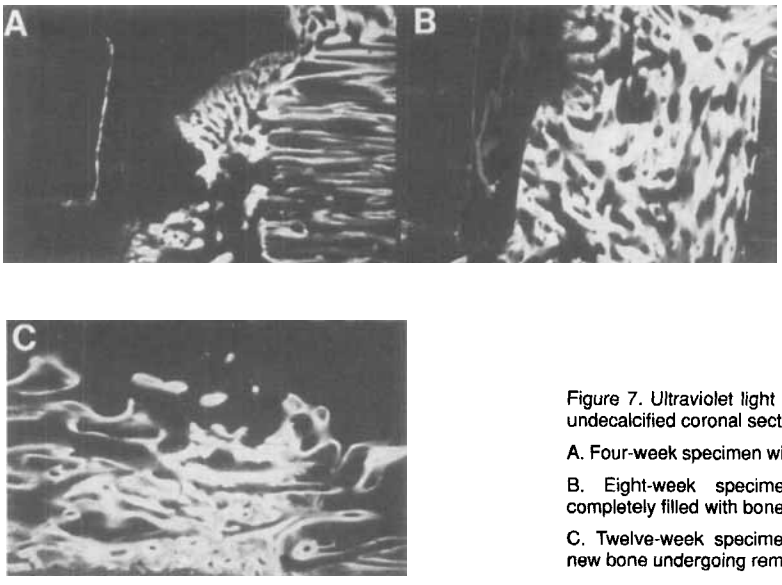

Figure 7. Ultraviolet light microscopy of 100 μm undecalcified coronal sections of gap, ×11.

A. Four-week specimen with gap filling with bone.

B. Eight-week specimen with gap almost completely filled with bone.

C. Twelve-week specimen with gap filled with new bone undergoing remodeling.

Table 2. Local properties of healing osteotomy. Mean *SEM*. (Markel et al. 1990a)

Weeks after surgery	Periosteal		Gap		Endosteal		Cortex	
Indentation stiffness (N/mm)								
2	38[a]	*11*	13[a]	*6*	31[a]	*7*	893[a]	*68*
4	49[a]	*8*	19[a]	*8*	8[a]	*11*	720[a,b]	*76*
8	198[b]	*14*	91[b]	*21*	99[b]	*30*	590[b]	*50*
12	138[c]	*24*	154[c]	*26*	40[a]	*8*	656[b]	*38*
Calcium content (mg calcium/g dry weight)								
2	170[a]	*19*	89[a]	*32*	179[a,b]	*13*	261[a]	*9*
4	156[a]	*10*	87[a]	*24*	166[a]	*16*	249[a]	*11*
8	232[b]	*6*	230[b]	*15*	220[b,c]	*9*	255[a]	*3*
12	255[b]	*13*	232[b]	*8*	232[c]	*24*	243[a]	*7*
New bone formation (%)								
2	39.9[a]	*5.9*	0.4[a]	*0.4*	25.0[a]	*3.9*	3.2[a]	*0.8*
4	63.4[b]	*2.4*	23.2[b]	*7.3*	42.4[b]	*3.6*	9.6[a]	*1.5*
8	58.5[b]	*2.2*	58.1[c]	*3.1*	35.2[b]	*2.3*	20.2[b]	*1.8*
12	59.6[b]	*2.5*	62.0[c]	*1.6*	13.0[c]	*2.9*	38.5[c]	*2.0*
Bone porosity (%)								
2	60.1[a]	*5.9*	99.6[a]	*0.4*	75.0[a]	*3.9*	11.5[a]	*1.0*
4	36.3[b]	*2.4*	76.8[b]	*7.3*	57.7[b]	*3.6*	22.3[b]	*1.2*
8	41.5[b]	*2.2*	41.9[c]	*3.1*	64.8[b]	*2.3*	21.3[b]	*3.8*
12	40.4[b]	*2.5*	38.0[c]	*1.6*	87.0[c]	*2.9*	16.7[c]	*2.1*

[a–d] Means within a column with superscripts of differing letters differed from each other ($p < 0.05$).

Noninvasive techniques' association with torsional properties

Ultimate torque

SPA, QCT, and DEXA of the gap tissue had the strongest associations with the ultimate torque of the bone. For SPA, DEXA, and MRI (T_1W), associations of gap tissue to ultimate torque were higher than for associations of torque with the other three tissues (Table 3). QCT and MRI (T_2W 2nd echo) of periosteal callus had the strongest associations with the ultimate torque of the bone. Correlations ranged from insignificant associations with many of the cortical and endosteal values to 0.76 for SPA with gap tissue.

Table 3. Mean regression coefficients (R^2) of noninvasive techniques versus structural strength

Techniques	Periosteal	Gap	Endosteal	Cortex
Torsional property, ultimate torque				
MRI (T_1W)	NS [a]	0.45 [a,b]	NS [a,b]	NS [a]
MRI (T_2W 1st echo)	NS [a]	0.31 [a]	NS [a]	NS [a,b]
MRI (T_2W 2nd echo)	0.48 [b]	0.38 [a]	NS [a]	0.29 [b]
QCT	0.49 [b]	0.60 [b]	0.35 [b]	NS [a,b]
SPA	0.22 [a,b]	0.76 [a,b]	NS [a,b]	NS [a,b]
DEXA	0.23 [a,b]	0.51 [a,b]	0.21 [a,b]	NS [a,b]
Torsional stiffness				
MRI (T_1W)	0.14 [a]	0.43 [a,b]	NS [a]	NS [a]
MRI (T_2W 1st echo)	NS [a]	0.24 [a]	NS [a]	NS [a]
MRI (T_2W 2nd echo)	NS [a]	0.21 [a]	NS [a]	NS [a]
QCT	0.73 [b]	0.74 [c]	NS [a]	NS [a]
SPA	0.44 [c]	0.69 [c]	0.44 [b]	0.18 [a]
DEXA	0.41 [c]	0.53 [b,c]	0.31 [b]	0.20 [a]

[a–d] Means within a column with superscripts of differing letters differedt from each other ($p < 0.05$).
NS Not significant ($p > 0.05$).

Table 4. Mean regression coefficients (R^2) of noninvasive techniques versus local properties

Techniques	Periosteal	Gap	Endosteal	Cortex
Indentation stiffness				
MRI (T_1W)	0.16 [a]	0.50 [a,b,c]	0.34 [a]	NS [a]
MRI (T_2W 1st echo)	0.29 [a,b]	0.35 [a,b]	0.29 [a]	NS [a]
MRI (T_2W 2nd echo)	0.28 [a,b]	0.33 [a]	NS [a,b]	NS [a]
QCT	0.64 [c]	0.56 [b,c]	0.40 [a,b]	NS [a,b]
SPA	0.67 [b,c]	0.51 [c]	0.29 [b]	NS [a]
DEXA	0.73 [c]	0.37 [a,b,c]	0.30 [b]	NS [a]
Calcium content				
MRI (T_1W)	NS [a]	0.42 [a,b]	NS [a]	0.19 [a]
MRI (T_2W 1st echo)	NS [a]	0.27 [a]	NS [a]	NS [a]
MRI (T_2W 2nd echo)	NS [a]	0.21 [a]	NS [a]	NS [a]
QCT	0.53 [c]	0.61 [b,c]	0.14 [a]	NS [a]
SPA	0.16 [a,b]	0.69 [c]	0.16 [a]	NS [a]
DEXA	0.20 [b,c]	0.34 [a]	NS [a]	NS [a]

[a–d] Means within a column with superscripts of differing letters differed from each other ($p < 0.05$).
NS Not significant ($p > 0.05$).

Torsional stiffness

QCT, SPA, and DEXA of the gap tissue had the strongest associations with the torsional stiffness of the bone (Table 3). QCT of periosteal callus had the strongest association with the torsional stiffness of the bone followed by DEXA and SPA. SPA and DEXA of endosteal callus had the strongest associations with torsional stiffness. For all techniques, gap tissue values had stronger associations than for the other three tissues. Correlation coefficients were as high as 0.74 for QCT of gap tissue.

Angular deformation at failure

There were no differences between the noninvasive techniques and their associations with angular deformation at failure for periosteal, endosteal, and cortical tissue. In gap tissue, QCT had a stronger correlation than the other techniques. Associations were insignificant for all techniques with all tissues except for QCT with gap tissue ($R^2 = 0.43$).

Energy absorption at failure

There were no differences between the noninvasive techniques and their associations with energy absorption at failure. Associations were insignificant for most correlations but ranged up to 0.60 for MRI (T_1W).

Noninvasive techniques' association with local properties

Indentation stiffness

QCT, DEXA, and SPA of periosteal callus had the strongest associations with indentation stiffness (Table 4). For gap tissue, SPA and QCT had the strongest associations. For endosteal callus, MRI (T_1W) and MRI (T_2W 1st echo) had the strongest associations. Techniques did not differ from each other for cortical tissue or if all tissues were combined. Correlations ranged from insignificant associations with many of the cortical values to 0.73 for DEXA with periosteal callus.

Calcium content

QCT and DEXA had the strongest associations with periosteal callus calcium content (Table 4). For gap tissue, QCT and SPA had the strongest associations. For endosteal callus and cortical tissue, no technique had a stronger association than the others. Correlations ranged from insignificant associations with many of the cortical values to 0.69 for SPA with calcium content of gap tissue.

Discussion

The strongest correlations between torsional properties and the noninvasive techniques were between ultimate torque and torsional stiffness, and SPA, QCT and DEXA. Correlations with energy absorption at failure and angular deformation at failure were poor or insignificant. There have been many studies which have demonstrated the poor ability of energy absorption at failure and angular deformation at failure to quantify bone healing (Aro et al. 1989, Lewallen et al. 1984, Rand et al. 1981).

Generally, gap tissue correlations were stronger than periosteal or endosteal callus correlations, especially for SPA and DEXA. As the gap remodels, it should ultimately regain the calcium content and density of normal cortical bone, and therefore, should correlate strongly with torsional properties of the bone. In contrast, periosteal and endosteal callus is formed to stabilize the bone ends and fill the gap with bone (Beljan et al. 1971, Eriksson et al. 1989, Sevitt 1980) and early in the course of fracture healing would be expected to be more strongly associated with the torsional properties of the bone (Markel et al. 1990a). As the bone heals, periosteal and endosteal callus is resorbed, therefore should be less closely associated with torsional properties later in the course of fracture healing.

Whether examining torsional or local properties of healing bone, QCT, SPA and DEXA usually had stronger associations than the three MRI sequences. The reasons for the relatively poor performance of MRI in this study are many. First, MR is only indirectly proportional to mineral density so would not be expected to have high correlations with calcium content (Nixon 1987). Second, MR has only rarely and unsuccessfully been used as a quantitative method; Jenkins et al. (1989) measured T_1 and T_2 relaxation times of vertebral bodies and could not distinguish between age, sex, or location in the spine. The technique's potential sources of error are many and include: 1) positioning of the region of interest, since large errors can result from small changes in position (Jenkins et al. 1989); 2) slice thickness limitations of 5 mm in this study; 3) edge effects at interfaces between low and high signal intensity, such as cortical bone and endosteal callus (Clark and Kelly 1988); 4) chemical shift between interfaces of fat-bound protons bordering hydrated tissues such as endosteal callus and trabecular bone; 5) focal field inhomogeneity from irregularly deposited calcium within the callus; 6) volume averaging of two opposing tissue planes with markedly different signal characteristics such as cortical bone and periosteal or endosteal callus; and 7) pulse imperfections of the hardware (Majumdar et al. 1986). Of the techniques examined in this study, MRI almost universally had the poorest correlations with the various parameters examined.

QCT, SPA, and DEXA had the strongest correlations with indentation stiffness of periosteal tissue. SPA and DEXA would be expected to have higher correlations with periosteal tissue than with other tissues since the thickness of the outer circumference of periosteal callus remains fairly constant at the periosteal sampling sites (Markel et al. 1990b). Therefore, changes in bone mineral content reflect, more directly, changes in calcium content rather than a combination of calcium content and tissue volume. The highest correlations were for periosteal callus ranging

as high as $R^2 = 0.73$ for DEXA. The reasons for poor correlations of SPA and DEXA with endosteal callus and cortical bone are many. The poor association of these techniques with cortical bone is probably due to the small change in cortical calcium content during the twelve-week study period, decreasing the variability of this parameter and lowering the regression coefficient. The explanation for the lack of correlations with endosteal callus is probably related to the two-dimensional technique's inability to directly measure within a three-dimensional structure. In contrast, QCT, through its tomographic technique, can directly measure trabecular bone (Cann 1988).

QCT has been shown to be accurate and precise in previous studies (Cann 1988). In this study, the short-term precision error of measuring calibration solutions ranged from 1.4 to 4.7 percent, which is well within the range reported by Rueggsegger et al. (1974) and Genant and Boyd (1977). The precision error associated with in vivo bone measurements were much higher, ranging as high as 27 percent for endosteal callus. Our inability to precisely measure the exact same site of bone probably is related to our small sample size and the relatively large variation of mineral content within the tissues. This large variation has been seen in other studies examining the tibia (Mazess 1983) and radius (Hangartner and Overton 1982).

The high correlations of QCT with calcium content of periosteal callus ($R^2 = 0.53$) and gap tissue ($R^2 = 0.61$) are comparable to values reported by Rohloff et al. (1982), Laval-Jeantet et al. (1984), and Cann (1988). Previous studies have revealed similar correlations between bone mineral content and the mechanical properties of vertebrae (McBroom et al. 1985), femora (Alho et al. 1988), and tibiae (Hvid et al. 1987). Correlations between bone mineral content and structural strength ranged as high as $R^2 = 0.82$ (McBroom et al. 1985). Most correlation coefficients ranged between 0.3 and 0.8. In this study, correlations with QCT were as high as 0.64 for local stiffness and 0.74 for torsional stiffness, comparable to or better than many of the previously mentioned studies.

SPA is both precise and accurate (Mazess 1983) and has been used to quantitate bone mechanical properties and bone healing (Leichter et al. 1982, Markel et al. 1990b). Correlation coefficients in this study ranged as high as 0.67 for correlations with indentation stiffness and 0.69 for correlations with torsional stiffness. These values are comparable to those of previous studies (Borders et al. 1977, Cann 1988, Leichter et al. 1982).

DEXA is precise and accurate (Sartoris and Resnick 1989, Wahner et al.1988). Correlations with calcium content were relatively poor in this study with 0.34 as the highest value. Correlations with mechanical properties were better than with calcium content, reaching 0.73 for indentation stiffness and 0.53 for the torsional stiffness of the bone (Markel et al. 1990b).

This study supports the concept of using noninvasive methods to determine the structural strength and local properties of bone, and specifically in this study, healing bone. QCT, SPA, and DEXA appear to have the greatest promise for this application. The prediction of the ultimate torque of the healing bone would appear to have the most interesting clinical applications since this parameter should have a close relationship with the risk of refracture after removal of the fixation or fracture in patients with bone tumors.

Acknowledgement

This study was supported by NIH grant AR08045 and a grant from EBI/Orthofix.

References

Alho A, Husby T, and Høiseth A. Bone mineral content and mechanical strength. Clin Orthop 1988; 227: 292–7.

Aro H T, Wahner H W, Kelly P J, Chao E Y S. Comparison of stable transverse and unstable oblique osteotomy healing in the canine tibia under external fixation. Trans Orthop Res Soc 1989; 14: 121.

Baron R, Vignery A, Neff L, Silverglate A, Maria A S. Processing of undecalcified bone specimens for bone histomorphometry. In: Bone Histomorphometry Techniques and Interpretation (Ed. Recker R). CRC Press, Inc. Boca Raton, FL 1979: 13–35.

Beljan J R, Hellewell A B, Goldman M. The effect of calcium deficiency on healing of experimental fractures in the avian tarsus as determined by the fracture repair ratio. Clin Orthop 1971; 78: 277–85.

Borders S, Peterson D R, Orne D. Prediction of bending strength of long bones from measurements of bending stiffness and bone mineral content. J Biomech Engrg 1977; 99: 40–4.

Budsberg S C, Verstraete M C, Soutas-Little R W. Force plate analysis of the walking gait in healthy dogs. Am J Vet Res 1987; 48: 915–8.

Burstein A H, Frankel V H. A standard test for laboratory animal bone. Technical note. J Biomech 1971; 4: 155–8.

Cann C E, Genant H K, Kolb F O, Ettinger B. Quantitative computed tomography for prediction of vertebral fracture risk. Metab Bone Dis Relat Res 1985; 6: 1–7.

Cann C E. Quantitative CT for determination of bone mineral density: A review. Radiology 1988; 166: 509–22.

Clark J A, Kelly W M. Common artifacts encountered in magnetic resonance imaging. Radiol Clin North Am 1988; 26: 893–920.

Eriksson S A V, Isberg B O, Lindgren J U. Prediction of vertebral strength by dual photon absorptiometry and QCT. Calcif Tiss Int 1989; 44: 243–50.

Falkenberg J. An experimental study of the rate of fracture healing. Acta Orthop Scand 1961; Suppl. 50.

Frost H M. Bone histomorphometry: Choice of marking agent and labeling schedule. In: Bone Histomorphometry Techniques and Interpretation (Ed. Recker R). CRC Press, Inc. Boca Raton, FL 1979: 38–57.

Genant H K, Boyd D P. Quantitative bone mineral analysis using dual-energy computed tomography. Invest Radiol 1977; 12: 545–51.

Hangartner T N, Overton T R. Quantitative measurement of bone density using gamma-ray computed tomography. J Comput Assist Tomogr 1982; 6: 1156–62.

Harris W H, LaVorgna J, Hamblen D L, Haywood E A. The inhibition of ossification in vivo. Clin Orthop 1968; 61: 52–60.

Hvid I, Bentzen SM, Jorgensen J. Axial compressive strength of trabecular bone at the proximal tibia assessed by quantitative computed tomography. Trans Orthop Res Soc 1987; 12: 52.

Jenkins J P R, Stehling M, Sivewright G, Hickey D S, Hillier V F, Isherwood I. Quantitative magnetic resonance imaging of vertebral bodies: A T1 and T2 study. Magn Reson Imaging 1989; 7: 17–23.

Jowsey J, Kelly P J, Riggs B L, Bianco A J, Scholz D A, Gershon-Cohen J B. Quantitative microradiographic studies of normal and osteoporotic bone. J Bone Joint Surg (Am) 1965; 47: 785–806.

Kelly P J, Peterson L F A, Janes J M. A method of using sections for microangiography for subsequent histologic study. Proc Staff Mtg Mayo Clin 1959; 34: 274–83.

Laval-Jeantet AM, Cann CE, Roger B, Dallant P. A post-processing dual-energy technique for vertebral CT densitometry. J Comput Assist Tomogr 1984; 8: 1164–7.

Leichter I, Margulies J Y, Weinreb A, Mizrahi J, Robin B C, Conforty B, Makin M, Bloch B. The relationship between bone density, mineral content, and mechanical strength in the femoral neck. Clin Orthop 1982; 163: 272–81.

Lewallen D G, Chao E Y S, Kasman R A, Kelly P J. Comparison of the effects of compression plate and external fixators on early bone-healing. J Bone Joint Surg (Am) 1984; 66: 1084–91.

Lewallen D G, Aro H T, Chao E Y S, Berquist T H, Kelly P J. Noninvasive evaluation of bone healing using quantitative MRI imaging. Trans Orthop Res Soc 1988; 13: 409.

Majumdar S, Orphanoudakis S C, Gmitro A, O'Donnell M, Gore J C. Errors in the measurements of T2 using multiecho MRI techniques. Magn Reson Imaging 1986; 3: 395–417.

Markel M D, Wikenheiser M A, Chao E Y S. A study of fracture callus material properties: Relation to the torsional strength of bone. J Orthop Res 1990a (in press).

Markel M D, Wikenheiser M A, Morin R L, Lewallen D G, Chao E Y S. The determination of bone fracture properties by dual-energy x-ray absorptiometry and single-photon absorptiometry. Calcif Tiss Int 1990b (in press).

Mazess R B. Noninvasive bone measurements. In: Skeletal Research II (Ed. Kunin A) Academic Press, Inc. New York, 1983: 277–343.

McBroom R J, Hayes W C, Edwards W T, Goldberg R P, White A A. Prediction of vertebral body compressive fracture using quantitative computed tomography. J Bone Joint Surg (Am) 1985; 67: 1206–14.

Mosekilde L, Mosekilde L. Normal vertebral body size and compressive strength: Relations to age and to vertebral and iliac trabecular bone compressive strength. Bone 1986; 7: 207–12.

Nixon D E, Moyer T P, Johnson P, McCall J T, Ness A B, Fjerstad W H, Wehde M B. Routine measurement of calcium, magnesium, copper, zinc, and iron in urine and serum by inductively coupled plasma emission spectroscopy. Clin Chem 1986; 32: 1660–5.

Nixon J R. Basic principles and terminology. In Magnetic Resonance of the Musculoskeletal System (Ed. Berquist T H, Ehman R L, Richardson M L). Raven Press, New York, 1987: 1–21.

Rand J A, An K N, Chao E Y S, Kelly P J. A comparison of the effect of open intramedullary nailing and compression-plate fixation on fracture-site blood flow and fracture union. J Bone Joint Surg (Am) 1981; 63: 428–42.

Rohloff R, Hitzler H, Arndt W, Frey K W, Lissner J. Influence of fat content of bone marrow on bone mineral measurement by CT and photon absorptiometry in trabecular bones. J Comput Assist Tomogr 1982; 6: 212–3.

Ruegsegger P, Niederer P, Anliker M. An extension of classical bone mineral measurements. Ann Biomec Eng 1974; 2: 194–205.

Sartoris D J, Resnick D. Dual-energy radiographic absorptiometry for bone densitometry: Current status and perspective. AJR 1989; 152: 241–6.

Sevitt S. Healing of fractures in man. In: Scientific Foundations of Orthopedics and Traumatology (Ed. Owen R, Goodfellow J, Bullough P). WB Saunders Co. Philadelphia 1980: 258–72.

Vanderhoeft P J, Kelly P J, Peterson L F A. Determination of growth rates in canine bones by means of tetracycline-labeled patterns. Lab Invest 1967; 11: 714–26.

Wahner H W, Riggs B L, Beabout J W. Diagnosis of osteoporosis: Usefulness of photon absorptiometry at the radius. J Nucl Med 1977; 18: 432–7.

Wahner H W, Dunn W L, Brown M L, Morris R L, Riggs B L. Comparison of dual-energy x-ray absorptiometry and dual photon absorptiometry for bone mineral measurements of the lumbar spine. Mayo Clin Proc 1988; 63: 1075–84.